Geophys. J. Int. (2004) **159,** 207–211 doi: 10.1111/j.1365-246X.2004.02367.x

Rupture process of the 1999 November 12 Düzce (Turkey) earthquake deduced from strong motion and Global Positioning System measurements

M.-P. Bouin,[1] M. Bouchon,[2] H. Karabulut[3] and M. Aktar[3,4]

[1] *Département de Sismologie, UMR* 7580, *Institut de Physique du Globe de Paris, France. E-mail: bouin@ipgp.jussieu.fr*
[2] *Université Joseph Fourier, LGIT, Grenoble, France*
[3] *Boğaziçi University, Kandilli Observatory and Earthquake Research Institute,* 81220 *Çengelköy, Istanbul, Turkey*
[4] *Tubitak, MRC, Gebze, Turkey*

Accepted 2004 April 8. Received 2004 April 8; in original form 2003 March 31

SUMMARY

We use the strong motion data recorded at near-fault accelerometers combined with Global Positioning System (GPS) measurements to infer the space and time evolution of the $M_w = 7.2$ 1999 November 12 Düzce (Turkey) earthquake. We confirm that the rupture is subshear towards the west whereas it overpassed the shear speed towards the east. The mechanism of the earthquake is predominantly right lateral on a 65° north-dipping fault. The strike-slip we infer represents at least 75% of the total seismic moment. We stress that the use of strong motion data allows us to constrain a strong spatial variation of the slip direction during faulting: to the west of the hypocentral region, the slip is oblique accompanied by a significant normal component. In the central and eastern part of the activated fault the slip is almost pure right lateral. This result is consistent both with the surface offset observations and with the long-term morphology of the fault. Neither strong motion data nor GPS data can resolve the complexity of the eastern termination of the Düzce rupture.

Key words: earthquake kinematics, GPS measurements, rupture process, strong ground motion.

INTRODUCTION

On 1999 November 12 an earthquake of magnitude $M_w = 7.2$ struck a segment of the North Anatolian Fault (NAF), eastward of the rupture zone of the 1999 August 17, $M_w = 7.4$, Izmit earthquake that occurred 3 months earlier. A 40 km long surface break was observed along the east–west Düzce Fault, and right lateral surface-slip up to 5 m has been documented (Akyüz *et al.* 2002). Significant vertical slip up to 3.5 m was observed near the western end of the activated segment, along the 5 km oblique normal fault bounding Eften Lake (Akyüz *et al.* 2002; Çakir *et al.* 2003).

Focal mechanism solutions of the Düzce earthquake indicate a north-dipping fault with dominant right lateral strike-slip motion and a small component of normal slip (see focal mechanism determinations from Harvard University, US Geological Survey and GFZ Potsdam). The mainshock (40.82° N, 31.186° E, Kandilli Observatory) located 3.5 km southeast of Düzce (see Fig. 1) at a depth of 12 km also indicates a north-dipping fault in agreement with the aftershock distribution (see Fig. 1) (Özalaybey *et al.* 2000).

This earthquake has been well-studied from geodetic (Ayhan *et al.* 2001; Bürgmann *et al.* 2002; Çakir *et al.* 2003) and teleseismic data (Yagi & Kikuchi 1999) to provide source tomographies. The strike-slip distribution provided by each of these studies is consistent: it is very simple with a single broad strike-slip maximum about the earthquake hypocentre (Yagi & Kikuchi 1999; Ayhan *et al.* 2001; Bürgmann *et al.* 2002; Çakir *et al.* 2003). When considered, normal slip is characterized by a distribution scattered on the fault plane, and is quite different (Ayhan *et al.* 2001; Bürgmann *et al.* 2002).

P- and *S*-wave arrival times picked on the near-source strong motion records have been already interpreted by Bouchon *et al.* (2001) to constrain the rupture velocity during the earthquake. Nevertheless the strong motion waveforms have not yet been analysed to retrieve the details of the rupture process. In this paper, we address the rupture history of the Düzce earthquake using the strong ground motions (SM) recorded close to the fault plane. The small number of near source SM data available (four) and the location of the SM stations beyond the terminations of the activated fault require the use of independent data to constrain the solution during the inversion procedure. We thus combine the Global Positioning System (GPS) measurements with the SM data to retrieve the space and time evolution of the Düzce rupture.

DATA SET

The SM station distribution (see Table 1) is shown in Fig. 1. Three accelerometers are located close to the fault plane activated by the

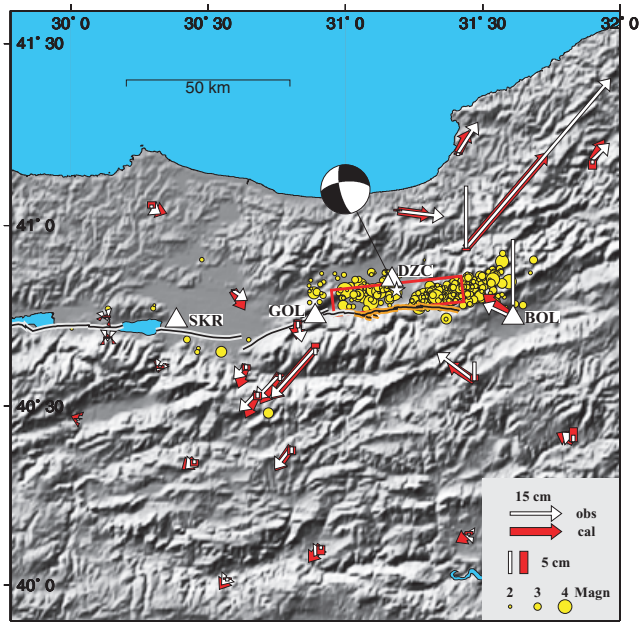

Figure 1. Map of the Düzce region. Düzce aftershocks are plotted as yellow circles (Özalaybey *et al.* 2000). The surface rupture of the Düzce earthquake is plotted as a black line highlighted in orange (Akyüz *et al.* 2002). The coseismic GPS observations from Bürgmann *et al.* (2002) are represented by white arrows and white bars (for horizontal and vertical displacements respectively), the displacements predicted by the model are represented by red arrows and red bars. The white star indicates the location of the epicentre, the white triangles stand for the accelerometric stations and the red rectangle represents the projection on the surface of the theoretical fault plane used in this study. The mechanism is the one deduced in this study.

Table 1. Strong motion stations.

Station	Acc.	Owner	Lat. (deg)	Long. (deg)
DZC (Düzce)	SMA-1	GDDA	40.8500	31.170
SKR (Sakaria)	GSR-16	GDDA	40.7370	30.384
BOL (Bolu)	GSR-16	GDDA	40.7470	31.610
GOL (Golyaka)	CMG-5	TN	40.7490	30.8891

GDDA, General Directorate of Disaster Affairs; TN, temporary network.

Düzce earthquake: DZC and BOL belong to the General Directorate of Disaster Affairs (GDDA), GOL was set up a few hours before the mainshock by a French–Turkish team. The fourth station, SKR, also belonging to the GDDA, is located 65 km away from the hypocentre.

The stations are installed on different geological settings: GOL is set up on the gouge of the fault where the rocks are expected to be highly deformed. DZC lies in the Düzce Sedimentary Basin and BOL is in the Bolu Basin. However, the travel path from the fault to BOL is mostly across a mountainous region. An initial investigation clearly pointed out the need to take into account local site information. As a result, we consider different velocity models for each station (Table 2).

The SM records integrated into velocity are displayed in Fig. 2. As shown in this figure, the waveforms are quite complex. For the westernmost and farthest site, SKR, the records are dominated by a surface wave with a period of about 10 s. The ground velocity at BOL is characterized by a short signal duration (about 10 s), a high-frequency content and a late energetic high-frequency phase arriving 5.3 s after *P* arrival on the east–west component. However, the ground displacement at this site, obtained by the double integration of the acceleration traces, is very simple as shown in Fig. 3. The quality of the analogue records at DZC and the 20 s high-pass filter of the instrument at GOL prevent us from obtaining the displacement at these sites.

Coseismic GPS data are from Bürgmann *et al.* (2002) and we refer to that article for details relating to the processing, resolution and analysis of GPS data. Displacements at BOL are the peak displacements obtained by double integration of the acceleration records. The 23 GPS stations are plotted in Fig. 1.

Table 2. Velocity models. Depth of the upper layers and corresponding *P* and *S* velocities. Below, the upper crust (32 km thick) is assumed to be uniform with *P* and *S* velocities of 6 km s^{-1} and 3.46 km s^{-1} respectively, increasing to 6.3 km s^{-1} and 3.64 km s^{-1} below 16 km. *P* and *S* velocities below the Moho are 8 km s^{-1} and 4.6 km s^{-1} respectively.

Station	Depth (km)	V_P (km s^{-1})	V_S (km s^{-1})
SKR	0.0–1.5	3.0	1.5
GOL	0.0–2.0	4.0	2.0
	2.0–4.0	5.0	2.8
DZC	0.0–2.0	4.0	2.0
BOL	0.0–0.2	4.0	2.3

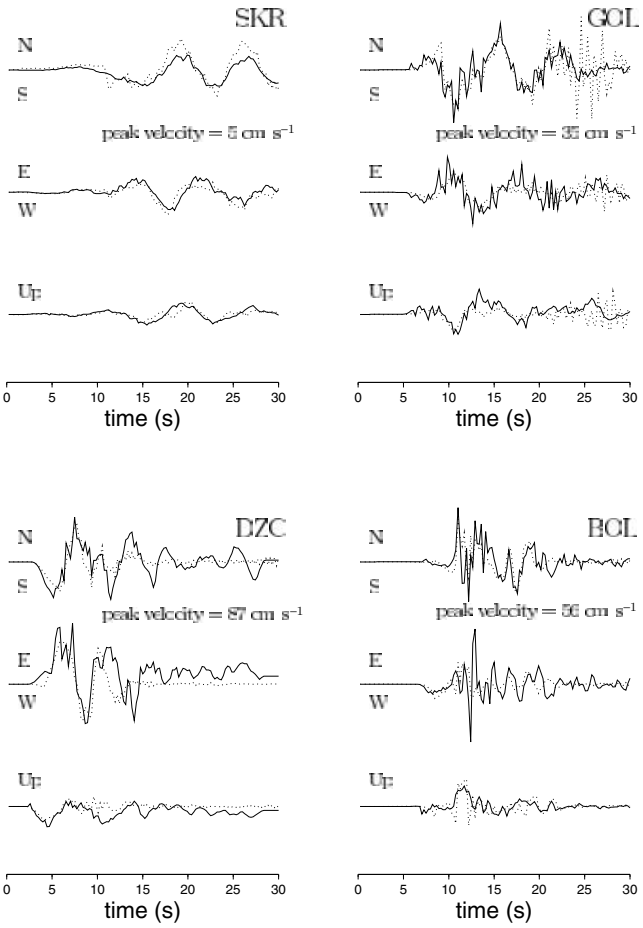

Figure 2. Ground velocities recorded (black line) at the four selected stations and calculated (dotted line) with the model displayed in Fig. 4. The amplitudes are normalized at each station. The numerical values indicated give the peak amplitude of the observed velocities. The arrival time of the *P* waves is indicated.

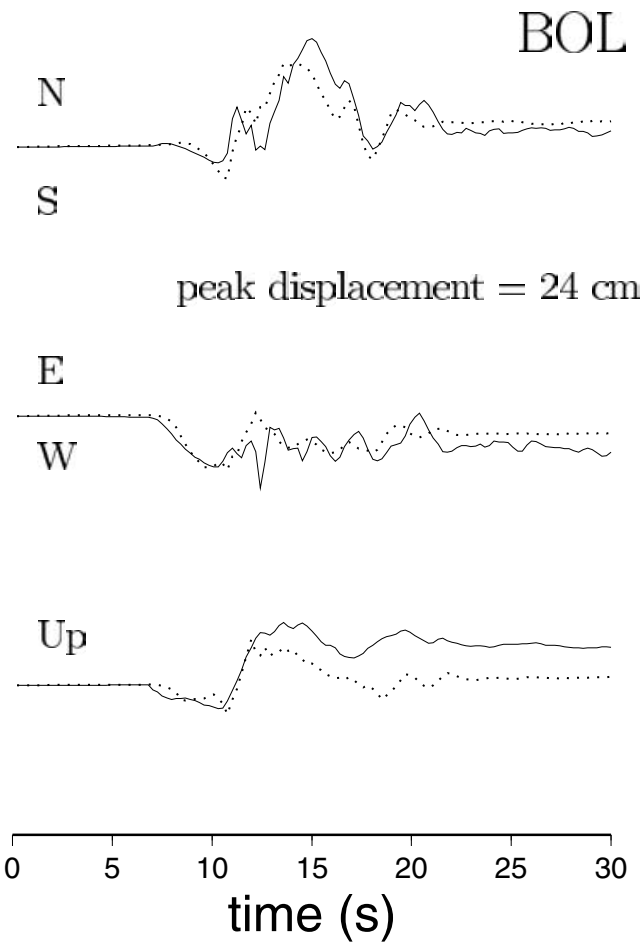

Figure 3. Ground displacement recorded (black line) at BOL and calculated (dotted line) with the model displayed in Fig. 4. The amplitudes are normalized. The numerical value indicated gives the peak amplitude of the observed displacement.

MODEL PARAMETERS AND INVERSION PROCESS

The method we employ in this study is that used by Bouchon *et al.* (2000) for the Izmit earthquake. We model the earthquake as a rupture which starts at the hypocentre and propagates radially on the fault. Slip at any location on the fault is assumed to grow as a ramp function starting at the arrival of the rupture front. The synthetics are computed using the discrete wavenumber method (Bouchon 1981) and an inversion scheme based on simulated annealing (Courboulex *et al.* 1996) is used to sample the model space. The fault is discretized into eight elements along the strike and four elements along the dip resulting in 32 subelements of 5 × 5 km. To compute synthetics, each element is represented by 25 double-couple point sources. The slip and the rise time of each element as well as the average westward rupture velocity constitute the space of the model parameters. Causality is required.

As has already been pointed out by Bouchon *et al.* (2001), a supershear rupture velocity toward the east is required by the short $S - P$ time (3.95 s) observed at BOL. The epicentral distance at this station is 39 km leading to a theoretical $S - P$ time of 4.7–4.8 s. The average rupture velocity inferred from the shear arrival is 4.1 km s^{-1} . This value is different from the one obtained by Bouchon *et al.* (2001) since an updated and refined hypocentre location is used here.

The fault geometry is inferred from the observed surface breaks (Akyüz *et al.* 2002). It consists of a unique segment over 40 km, striking 265°N, dipping 65° to the north and extending from the surface to a depth of 20 km (Fig. 1).

We performed tests to assess the sensitivity of the SM data to the dip angle. Our initial assumption of a vertical fault model provides a good fit to the records on the transverse components (i.e. the north–south component) at BOL, SKR and GOL but fails to model the records on the normal components. A north-dipping fault is clearly needed to explain the signal on the normal component at those stations. As a result, we repeat the inversion for dip angles ranging from 90° to 60°. The best results are obtained for a dip angle of 65° which we used in this study. A lower angle is not compatible with the SM data.

The best fit is determined by the minimization of the cost function:

$$S = \sum_{k=1}^{4}\sum_{j=1}^{3}\sum_{i=1}^{N}[(Csm_{kj}(i) - Osm_{kj}(i))]^2/4 + \sum_{k=1}^{23}\sum_{j=1}^{3}[(Cgps_{kj} - Ogps_{kj})]^2/23$$

where $Csm_{kj}(i)$ and $Osm_{kj}(i)$ are respectively, the calculated and observed ground velocities j at station k and time i, $Cgps_{kj}$ and $Ogps_{kj}$ respectively, the observed and calculated GPS displacements j at station k. N is selected as 85 points representing 20 s of signal, except at station SKR where 30 s of signal is considered. All the time-series start at the origin time of the earthquake except for SKR, for which the distance from hypocentre is the longest. No filtering is applied to the data.

Following Bouchon *et al.* (2002), we average 10 best models obtained from the inversion performed using different initial parameters. This allows a smoothing directly linked to the spatial resolution of the parameters. This image is presented in Fig. 4.

In Fig. 1 we present observed and calculated GPS vectors. As shown in the figure, the overall fit of the horizontal GPS measurements is good in amplitude and direction. There is an underestimation of the amplitude at the station with the largest displacement. However, Çakir *et al.* (2003) suggest that measurement at this station may have significant errors. At the three stations closest to the fault at the eastern side horizontal fit is not as good as for the other stations and the model fails to reproduce the vertical displacement. At the other stations, the vertical component of the GPS signal is small for this earthquake and it is well reproduced by the model.

In Fig. 2, we present synthetic and observed waveforms. The long-period velocity recorded at SKR is well fitted by the synthetics. At GOL, the low-frequency part of the signal is well reproduced for the three components. At DZC, the ground velocity calculated with the model provides a reasonably good fit for the first few seconds, except that the deflection associated with the P wave on the east–west component has the reverse polarity. DZC is an analogue station and the records are manually digitized. The integration process is less stable for this station and we do believe that this deflection reflects a noise effect linked to the data processing rather than a signal effect.

At BOL, the southwest deflection of the recorded velocity associated with the P wave is well reproduced by the synthetics. The latter part of the recorded signal is difficult to compare with the synthetics because of its high-frequency content. In Fig. 3, we compare the ground acceleration integrated into displacement at BOL with the displacement predicted by the model. Although the ground

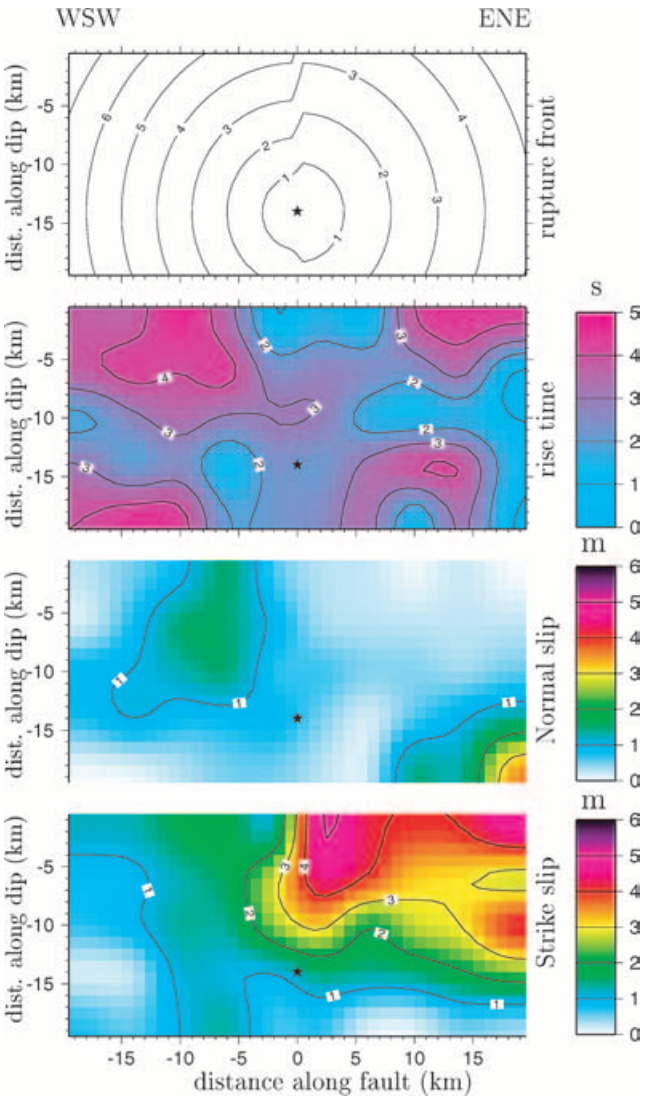

Figure 4. From top to bottom: images of the rupture front (1 s of interval from the beginning of the rupture), rise time, normal slip and horizontal slip on the fault. The black star indicates the position of the hypocentre.

displacement was not directly inverted, it is very well fitted by the synthetics calculated with the supershear rupture velocity.

RUPTURE HISTORY

As shown in Fig. 4, strike-slip and normal slip distributions do not correlate. This pattern is a remarkably robust feature of inversions performed with SM alone or with SM and GPS data. Strike-slip is larger on the eastern portion on the fault but it remains significant on the western portion. On the contrary normal slip is concentrated on the western part of the fault whereas it is close to zero in the eastern one except in the deep part. This slip distribution agrees with the surface-slip distribution observed along the surface break.

Specifically, the largest strike-slip reaches 5 m on the central and eastern part of the fault mainly at shallow depths, from 10 km to the surface. This is consistent with the right-lateral offset observed at the surface for which the maximum value is measured in the epicentral region and is 5 m (Akyüz *et al.* 2002). This large strike-slip area is well constrained both by the SM and the GPS data set. The inversions performed using SM data alone show that SKR records are sensitive to the overall slip distribution pattern and allow the inversion process to stabilize. The slip duration is relatively short, about 1.5–2 s, except for shallow depths at the eastern end of the fault where it lasted 4–4.5 s.

The normal slip we infer is concentrated a few kilometres to the west of the epicentre, (see Fig. 4) in a narrow zone (the eastern termination will be discussed later). It is distributed from the surface down to a depth of 12 km and reaches 2 m. It is spatially consistent with the zone where an impressive vertical uplift of up to 3.5 m was measured at the surface (Akyüz *et al.* 2002; Çakir *et al.* 2003). The slip duration is about 4–4.5 s. This area of large normal slip is required by SM data. GPS and InSAR data also required normal slip. The models of Ayhan *et al.* (2001) and Bürgmann *et al.* (2002) display significant vertical slip in this area. However, these data can also be fitted by a model with a constant rake on the fault plane (Ayhan *et al.* 2001; Bürgmann *et al.* 2002; Çakir *et al.* 2003). This shows that geodetic data are not constraining by themselves. The inversion using SM data alone clearly demonstrates that GOL and DZC records require normal slip. A pure strike-slip model fails to reproduce the data amplitude on the horizontal components at GOL and DZC as illustrated in Fig. 5. This is not surprising, as on SM records the largest amplitudes are radiated by the fault portion closest to the station; GOL and DZC are situated less than 20 km from the place where a large component of coseismic vertical slip has been observed in the field. We believe that the normal component of slip on this part of the fault is well resolved.

The model (Fig. 4) shows a slip distribution pattern which is different on the two terminations of the fault. Whereas the slip died off gradually to the west, both strike-slip at shallow depth and normal slip at greater depth remain significant at the eastern termination of the assumed fault plane. The aftershock distribution also displays a discrepancy between the western and the eastern part of the fault: as shown in Fig. 1, the aftershocks are distributed in two clear separated swarms (Özalaybey *et al.* 2000). One is located from the epicentral area to 25 km west and is clearly associated with the mapped surface rupture. The other swarm, separated from the previous one by a gap of aftershock activity, extends 10 km further east than the mapped surface breakages.

One may propose that the earthquake has broken an additional segment towards the east, beyond the observed surface rupture traces. The eastern cluster extends until the Bolu Mountain in a

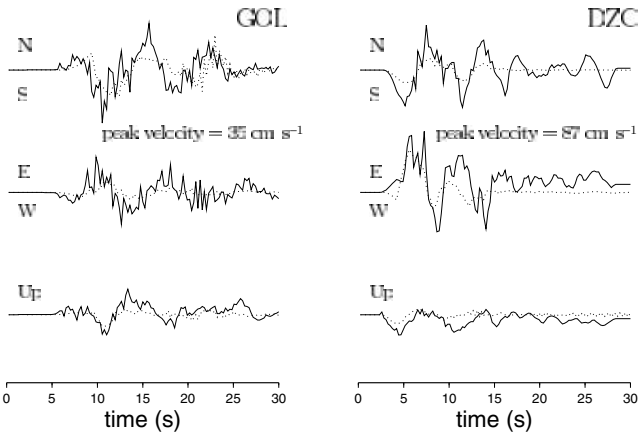

Figure 5. Ground velocities recorded (black line) at GOL and BOL stations and calculated (dotted line) with a model assuming pure strike-slip. The amplitudes are normalized at each station. The numerical values indicated give the peak amplitude of the observed velocities.

northeasterly direction whereas the fault system continues in the east–west direction to merge the single continuous strand of the NAF eastward. This might highlight such a segment and the extension of the rupture to the east. However, the clearly diffuse character of this aftershock swarm in cross-sectional view (Özalaybey *et al.* 2000; Çakir *et al.* 2003) prevents us from defining such a plane in depth. Assuming a longer fault to the east, by up to 10 km, would imply a source duration up to 3.5 s longer. Furthermore such a longer fault is not consistent with the data recorded at the station closest to the eastern termination (BOL). For that station the source duration is 10 s and the three-component SM records at BOL do not require a longer source duration. The maximum prolongation of the rupture to the east that the BOL SM data can tolerate is about 5 km. This is at best the spatial resolution of our model because this is the size of the subelement used in inversion.

Let us discuss the area of deep large normal slip at the eastern end of the rupture. This represents less than 5% of the total seimic moment of our model. Inversions performed using SM alone show that this normal slip is required by BOL records. The models of Ayhan *et al.* (2001) and Bürgmann *et al.* (2002) display significant normal slip on the eastern edge of the fault, at shallower depths. This suggests that such a normal dip at the eastern termination of the rupture is also required by the GPS data. Normal slip there is surprising, as no vertical slip associated with the surface breakage has been observed in that area. One can argue that a deep normal slip may not have reached the surface. Alternatively, this deep large normal slip might be another element, together with the aftershock distribution pattern to the east, suggesting that the nature of the eastern termination of the Düzce rupture is more complicated than is assumed in our model based on the observed surface break. The fact that the vertical displacements at the three GPS sites close to the eastern termination are not reproduced by our model reinforces such a hypothesis.

Previous analyses (Ayhan *et al.* 2001; Bürgmann *et al.* 2002; Çakir *et al.* 2003) have shown that the GPS data set does not have the resolution to constrain the eastern termination of the rupture. Clearly it is also beyond the resolution of the SM data set.

The average slip on the fault that we infer is about 2 m over a total length of rupture of 40 km. The total rupture duration is 8 s. Whereas this value is significantly shorter than the one obtained by teleseismic analysis of body waves (Yagi & Kikuchi 1999; Tibi *et al.* 2001), the seismic moment we infer, 5.26×10^{19} N m (corresponding to a moment magnitude of $M_{\mathrm{w}} = 7.1$) is consistent with previous analyses (Yagi & Kikuchi 1999; Tibi *et al.* 2001; Ayhan *et al.* 2001; Bürgmann *et al.* 2002; Çakir *et al.* 2003). The strike-slip represents 75% of the seismic moment yielding to the following mechanism: strike 265°, dip 65° (strike and dip are fixed) and rake −160° following the convention of Aki & Richards (1980). The mechanism plotted in Fig. 1 is in good agreement with previous focal mechanism determinations (see focal mechanism determinations from Harvard University and US Geological Survey) and teleseismic analysis (Tibi *et al.* 2001).

CONCLUSION

Analysis of the strong motion data recorded at near-fault accelerometers combined with the GPS measurements allows us to constrain some details of the space and time evolution of the Düzce earthquake. Specifically, we point out a strong rake variation during faulting: The major slip occurs in the central and eastern part of the fault, at shallow depth. It reaches 5 m of pure right lateral slip. To the west of the hypocentre, significant normal slip occurs in a narrow zone, from 12 km in depth to the surface. Its amplitude ranges between 1 and 2 m, that is the amplitude of the strike-slip in that area. This yields to an oblique mechanism with a significant normal component on this part of the fault. This is consistent with the long-term morphology of the fault that displays a sedimentary basin (the Düzce Basin) with a large swamp depression (Eften Lake) to the west of the epicentral region.

At the eastern termination of the fault, in depth, we suggest two scenarios that the data set used in this study does not allow us to discriminate: either the mechanism is once again oblique with a significant normal component or the fault geometry is different from the one deduced from the observed surface break.

ACKNOWLEDGMENTS

We are grateful to Semih Ergintav from TUBITAK-MAM for providing GPS data. This work has been performed within the framework of the collaborative programme on the seismic risk in the Istanbul and Sea of Marmara region coordinated by the Turkish TUBITAK and the French INSU-CNRS, with support from the French Ministry of Foreign Affairs (MAE). This is IPGP contribution 1981.

REFERENCES

Aki, K. & Richards, P., 1980. *Quantitative Seismology, Theory and Methods*, W.H. Freeman, San Francisco.

Akyüz, H.S., Hartleb, R., Barka, A., Altunel, E., Sunal, G., Meyer, B. & Armijo, R., 2002. Surface rupture and slip distribution of the 12 November 1999 Düzce earthquake (M 7.1), north Anatolian fault, Bolu, Turkey, *Bull. seism. Soc. Am.,* **92**(1), 61–66.

Ayhan, M.E., Bürgmann, R., McClusky, S., Lenk., O., Aktung, B., Herece, E. & Relinger, R. E., 2001. Kinematics of the $M_W = 7.2$, 12 November 1999, Düzce, Turkey, earthquake, *Geophys. Res. Lett.,* **28**(2), 367–370.

Bouchon, M., 1981. A simple method to calculate Green's functions in elastic layered media, *Bull. seism. Soc. Am.,* **72,** 745–757.

Bouchon, M., Toksöz, N., Karabulut, H., Bouin, M.P., Dietrich, M., Aktar, M. & Edie, M., 2000. Seismic imaging of the Izmit rupture inferred from the near-fault recordings, *Geophys. Res. Lett.,* **27**(18), 3013–3016.

Bouchon, M., Bouin, M.-P., Karabulut, H., Toksöz, N., Dietrich, M. & Rosakis, A. J., 2001. How fast is rupture during an earthquake? New insights from the 1999 Turkey earthquakes, *Geophys. Res. Lett.,* **28**(14), 2723–2725.

Bouchon, M., Toksöz, N., Karabulut, H., Bouin, M.P., Dietrich, M., Aktar, M. & Edie, M., 2002. Space and time evolution of rupture and faulting during the 1999 Izmit (Turkey) earthquake, *Bull. seism. Soc. Am.,* **92**(1), 256–266.

Bürgmann R. *et al.,* 2002. Deformation during the 12 November 1999 Düzce, Turkey, earthquake, from GPS and InSAR data, *Bull. seism. Soc. Am.,* **92**(1), 161–171.

Çakir, Z., Barka, A., de Chabalier, J.-B., Armijo, A. & Meyer B., 2003. Kinematics of the November 12, 1999 ($M_w = 7.2$) Düzce earthquake from SAR interferometry, *Turk. J. Earth Sci.,* **12,** 105–118.

Courboulex F., Virieux, J., Deschamps, A. Gibert, D. & Zollo, A., 1996. Source investigation of small event using empirical Green's function and simulating annealing, *Geophys. J. Int.,* **125,** 768–780.

Özalaybey, S., Aktar, M., Ergin, M., Karabulut, H., Bouchon, M., Tapirdamaz, C. & Yörük, A., 2000. Aftershocks studies following recent earthquakes in Turkey, *XXVII General Assembly of the European Seismological Commission (ESC), Book of Abstracts and Papers,* p. 31, Lisbon University, Lisbon, Portugal.

Tibi, R. *et al.,* 2001. Rupture process of the 1999 August Izmit and November 12 Düzce (Turkey) earthquakes, *Geophys. J. Int.,* **144,** F1–F7.

Yagi, Y. & Kikuchi, M., 1999. *Turkey Earthquake.* http://wwweic.eri.u-tokyo.ac.jp/yuji/trk2/Turkeyafter.html.